

# Journal of Materials Chemistry B

Accepted Manuscript



This is an *Accepted Manuscript*, which has been through the Royal Society of Chemistry peer review process and has been accepted for publication.

*Accepted Manuscripts* are published online shortly after acceptance, before technical editing, formatting and proof reading. Using this free service, authors can make their results available to the community, in citable form, before we publish the edited article. We will replace this *Accepted Manuscript* with the edited and formatted *Advance Article* as soon as it is available.

You can find more information about *Accepted Manuscripts* in the [Information for Authors](#).

Please note that technical editing may introduce minor changes to the text and/or graphics, which may alter content. The journal's standard [Terms & Conditions](#) and the [Ethical guidelines](#) still apply. In no event shall the Royal Society of Chemistry be held responsible for any errors or omissions in this *Accepted Manuscript* or any consequences arising from the use of any information it contains.

# Tunable Stellate Mesoporous Silica Nanoparticles for Intracellular Drug Delivery<sup>†</sup>

Cite this: DOI: 10.1039/x0xx00000x

Lin Xiong,<sup>a</sup> Xin Du,<sup>a</sup> Bingyang Shi,<sup>a</sup> Jingxiu Bi,<sup>a</sup> Freddy Kleitz,<sup>b</sup> and Shi Zhang Qiao\*,<sup>a</sup>

Received 00th January 2012,  
Accepted 00th January 2012

DOI: 10.1039/x0xx00000x

www.rsc.org/

Stellate mesoporous silica nanoparticles with special radial pore morphology were easily synthesized using triethanolamine as the base catalyst in a wide range of synthesis conditions. By adjusting surfactant composition, reaction temperature and time, and reagent ratio, the particle size of the material could be tailored continuously ranging from 50 to 140 nm and the pore size from 2 to 20 nm. By analyzing the effects of the different synthesis parameters, it is concluded that the particles are formed following a nucleation-growth mechanism and the reaction kinetics play an important role in determining the particle size and pore structure. These stellate MSNs can be conveniently functionalized with a nontoxic low molecular weight poly(ethylene imine) (PEI, 800 Da) by a delayed condensation method. The resulting nanocomposites not only possess auto-fluorescence for suitable particle tracking but also demonstrate good potential for intracellular delivery of the anticancer doxorubicin drug.

## 1. Introduction

Mesoporous silica nanoparticles (MSNs) have attracted great research interest because of their potential usage as drug delivery carriers.<sup>1,2</sup> For these sophisticated applications, a tight control over the particle size and the pore structure of the material is highly desirable. For example, the particle size of MSNs was reported to have an influence on the biodistribution,<sup>3</sup> cellular uptake,<sup>4</sup> nucleus entering<sup>5</sup> and biocompatibility<sup>6</sup> while the pore structure is related to the drug release profile<sup>7</sup> and loading capability<sup>8,9</sup> of MSNs. Therefore, considerable efforts have been made towards a precise control over the size and pore structure of MSNs.

To achieve passive accumulation of the drug carriers inside tumor tissues via the enhanced permeation and retention (EPR) effect,<sup>1</sup> a particle diameter between 30 nm and 150 nm is desired. Although nano-sized silica nanoparticles can be readily prepared following the Stöber method,<sup>10</sup> nano-sized MSNs were not successfully synthesized until about a decade ago, by controlling the reactant concentration<sup>11,12</sup> or adopting a dilution and quenching method.<sup>13</sup> Later, other studies showed that the particle size can be controlled by introducing a second surfactant<sup>14,15</sup> and/or co-solvent in the synthesis mixture.<sup>16</sup> More recently, particle size control through reaction pH adjustment was also demonstrated.<sup>4,17</sup> However, the preparation methods in these previous reports usually involved highly diluted solutions, which led to difficulties in scale-up and isolation of the products. By employing triethanolamine (TEA) as the base catalyst, Bein and coworkers succeeded to synthesize MSNs with particle diameter below 100 nm and narrow particle size distributions, this time from concentrated solutions.<sup>18</sup>

On the other hand, a large mesopore structure (pores > 5 nm) possesses several advantages such as high drug loading<sup>19</sup> and capability of loading large biomolecules,<sup>20</sup> e.g., proteins<sup>21</sup> or nucleic acids.<sup>22,23</sup> However, most of the reported pore sizes of MSNs are limited to 3-4 nm because of the commonly used surfactant template, cetyltrimethylammonium bromide (CTAB). Although using a pore swelling agent<sup>21</sup> or dual surfactants<sup>24</sup> can enlarge mesopores, these methods generally cannot guarantee maintaining uniform particles below 200 nm or require specific treatment such as prolonged hydrothermal process.<sup>25-27</sup> Therefore, it is still a challenge to combine the features of small particle size, narrow particle size distribution and large mesopores within one MSN system.

Very recently, Zhang et al. reported a facile procedure for synthesizing MSNs with size below 200 nm and mesopores up to 17 nm.<sup>28</sup> Furthermore, these MSNs possess special radial pore morphology, the so-called stellate pore morphology, and this kind of structure was reported to facilitate mass transport inside the pores.<sup>29,30</sup> From the view point of synthesis, this work can be seen as an derivatization of the previous synthesis method of Bein<sup>18</sup> in that, not only the base catalyst was exchanged from triethanolamine to several kinds of other small organic amines but also the standard CTAB surfactant was replaced by cetyltrimethylammonium tosylate (CTAT). Although the feasibility of using different catalysts and surfactants to control morphology and porous structure of the final particles has been explored, quantitative aspects of the synthesis protocol, such as the effects of using mixed surfactants, the ratio between reactants, reaction temperature and reaction time, must still be thoroughly substantiated and clarified. In this work, a significant influence of these factors on the final MSN products is demonstrated in a TEOS/CTAT/TEA/H<sub>2</sub>O system. We evidence that by tuning

these parameters, it is possible to easily adjust the pore structure and particle size of stellate MSNs over a wide range. Furthermore, the particle formation mechanism is studied by analyzing the products obtained under different synthesis conditions. Finally, the stellate MSNs are functionalized with low molecular weight poly(ethylene imine) (PEI), and the resulting nanocomposites demonstrate excellent potential for intracellular delivery of anticancer drug doxorubicin (DOX).

## 2 Materials and methods

### 2.1 Materials

Tetraethyl orthosilicate (TEOS), (3-Aminopropyl)-triethoxysilane (APTES), triethanolamine (TEA), cetyltrimethylammonium bromide, cetyltrimethylammonium tosylate, branched polyethylenimine (PEI, M.W.: 800 Da), glutaraldehyde (GA, 50 wt %), ethanol, dimethylsulfoxide (DMSO), 3-[4,5-dimethylthiazol-2-yl]-2,5-diphenyltetrazolium bromide (MTT), trypsin (0.25%) were purchased from Sigma Aldrich. Doxorubicin hydrochloride (DOX) was purchased from Beijing Huafeng United Technology Co., Ltd. Dulbecco's Modified Eagle's Medium (DMEM), fetal bovine serum (FBS), trypsin-EDTA, penicillin-streptomycin (PS) mixture, and phosphate buffered saline (PBS) were purchased from Gibco-BRL (Grand Island, USA). All chemicals were used as received without further purification.

### 2.2 Synthesis of MSNs

MSNs were synthesized using TEOS as the silica source, triethanolamine as the base catalyst, CTAT and/or CTAB as the structure-directing agent. According to the literature,<sup>28</sup> MSNs with stellate morphology are synthesized at 80 °C with a molar ratio of 1.0TEOS:0.06CTAT:0.026TEA:80.0H<sub>2</sub>O. Using that formula as a starting point, the variations in this study are summarized in Table 1 with the respective denotation and physical parameters of samples.

In a typical synthesis, a given amount of CTAT/CTAB and TEA was first dissolved in 25 ml DI water to form a clear solution at a pre-set reaction temperature. Then, 3.9 ml TEOS was quickly added to the solution and after a selected period of time the mixture was centrifuged at 16000 rpm for 15 min. The white precipitate was copiously washed with DI water, collected, and dried in oven at 60 °C for 24 h. After the particle synthesis, the surfactant template was removed by calcination at 550 °C for 6 h with a ramp rate of 0.5 °C/min in air, unless otherwise specified.

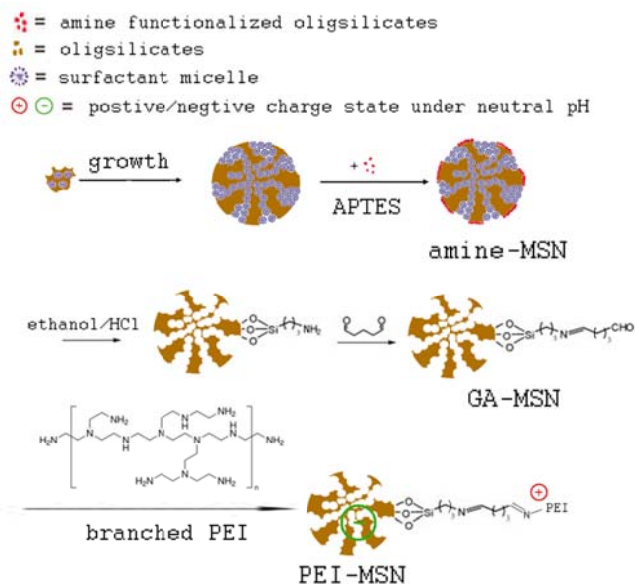
### 2.3 Functionalization of MSNs.

The functionalization process is presented in Scheme 1 and Fig. S1. Firstly, the delayed co-condensation method<sup>31</sup> was adapted to synthesize amine-modified MSNs (amine-MSN). The synthesis procedure is similar to the T10 sample except that a 200 μL mixture of TEOS and APTES (volume ratio 1:1) was added at 1 h after the reaction began at 80°C. After washing the amine-functionalized particles with ethanol and water, the CTAT surfactant was extracted for two times in a refluxing solution of hydrochloric acid (HCl) in ethanol (10% v/v) at 78 °C for 24 h. For glutaraldehyde (GA) conjugation, 50 mg of extracted particles were dispersed in 10 mL of sodium phosphate buffer (pH 7.4). Then 100 μL of glutaraldehyde (50 wt %) was added, and stirred at room temperature for 6 h. The glutaraldehyde modified MSNs (GA-MSN) were collected by centrifugation and washed intensively with ethanol for several times to remove excess glutaraldehyde. Afterwards, the particles were dispersed in 10 mL of PEI aqueous solution (0.5 mg/ml) and stirred at room temperature for 6 h. Finally, the suspension was centrifuged and the precipitate was washed with ethanol and dried to obtain PEI-modified MSNs (PEI-MSN). For comparison, unmodified MSNs (ex-MSN) were also prepared according to the synthesis procedure of T10, except that the CTAT surfactant was removed by extraction rather than calcination.

Table 1. Synthesis conditions and structural parameters\*.

Sample	Reactant ratio	temperature	time	Surfactant composition	Particle size	S <sub>BET</sub>	V <sub>t</sub>	V <sub>f</sub>
	(TEOS/surfactant /TEA /H <sub>2</sub> O mole ratio)	(°C)	(h)	(CTAT/CTAB mole ratio)	(nm)	(m <sup>2</sup> /g)	(cm <sup>3</sup> /g)	(cm <sup>3</sup> /g)
B10	1:0.06:0.026:80	80	2	10:0	45±5	689	1.14	0.47
T3B7				3:7	50±5	762	1.57	0.59
T5B5				5:5	60±5	717	1.46	0.62
T7B3				7:3	70±7	615	1.35	0.56
T9B1				9:1	95±9	602	1.37	0.57
T10 (T80)				110±12	581	1.36	0.51	
TC/2	1:0.06:0.013:80	95	2	10:0	130±9	375	1.00	0.37
TC/4	1:0.06:0.0065:80				140±13	424	0.88	0.38
TC/8	1:0.06:0.00325:80				–	427	1.32	0.44
TN	1:0.06:0:80				–	245	0.84	0.25
T95	1:0.06:0.026:80				108±10	454	0.77	0.43
T65					110±11	708	1.82	0.61
T50		80±7	788	1.71	0.69			
T50-24h	0.33:0.06:0.026:80	50	24	100±6	531	1.14	0.46	
TSi/3			2	70±8	885	2.16	0.97	

\* Particle sizes are estimated by averaging 50 particles from the SEM images. Total pore volumes (V<sub>t</sub>) and framework pore volumes (V<sub>f</sub>) were determined from N<sub>2</sub> adsorbed at P/P<sub>0</sub>=0.99 and P/P<sub>0</sub>=0.8, respectively.



Scheme 1 Synthesis scheme of amine and PEI functionalized MSNs.

## 2.4 DOX loading and release

For doxorubicin loading, 5 mg of MSNs were mixed with 5 ml of DOX solution in PBS (0.5 mg/mL) and stirred for 24 h under dark environment. Then, the nanoparticles were collected by centrifugation at 13500 rpm for 10 min. The precipitate was washed gently with PBS three times and dried at 60 °C. To evaluate the DOX loading efficiency, the supernatant and all the washing liquid fractions were collected, and the residual DOX content was determined using a standard curve by UV-vis adsorption at 480 nm. The release profile of DOX from MSNs was investigated at 37 °C in two different release media: (a) acetate buffer, pH 5.0; and (b) PBS, pH 7.4, using a dialysis bag diffusion technique. The DOX loaded particles (5 mg) were suspended in 5 mL release media in the dialysis membrane bag (MWCO ¼ 3500) and the bag was immersed in 15 mL release media and shaken at a speed of 100 rpm at 37 °C. The amount of DOX released at different time intervals was determined by UV-vis measurement at 480 nm.

## 2.5 Cell culture and cell viability

HeLa cells were grown in DMEM culture medium supplemented with 10% (v/v) FBS and penicillin/streptomycin (100 U/mL and 100 µg/mL, respectively) in a humidified 5% CO<sub>2</sub> atmosphere at 37 °C. For all experiments, cells were harvested by using 0.25% trypsin and resuspended in fresh medium before plating.

The viability of cells in the presence of MSNs was investigated using MTT assay. HeLa cells were seeded into 96-well plates at a density of  $1 \times 10^4$  per well in 100 µL of media and grown for 24 h. Then, the growth medium was replaced with 100 µL of cell culture medium containing different concentrations of MSNs with or without DOX loading. After incubation for 24 h, the medium was removed. Then 100 µL fresh medium and 10 µL MTT (5.0 mg/mL in PBS) were added to each well and the cells were further incubated for 4 h. After that, the growth medium was removed and 150 µL of DMSO was added to each well to ensure complete solubilization of formazan crystals. Finally, the absorbance was determined

using the Biotek Microplate Reader (Biotek, USA) at the wavelength of 570 nm. Data were expressed as mean ± standard deviation (SD) of four independent experiments. The viability of untreated cells was assumed to be 100%.

## 2.6 Confocal laser scanning microscopy (CLSM)

To check cellular uptake and auto-fluorescence of PEI-MSN, HeLa cells were seeded at a concentration of  $2 \times 10^5$  cells/well in a 6-well plate with one piece of cover glass at the bottom of each well and cultured for 24 h. PEI-MSN with or without DOX loading was then added to the incubation medium at the concentration of 50 µg/ml. After a desired period of time, the medium was removed. The cells were washed twice with PBS and fixed with 4 wt % formaldehyde. The cell nucleus was stained with Hoechst 33258 (2 µM) for 10 min at room temperature. After the incubation, the cells were softly washed twice to remove excessive Hoechst 33258. At last, 2 mL of PBS was added and the cover glass was visualized under a confocal laser scanning microscope (Leica Confocal 1P/FCS). Optical sections were averaged 4 times to reduce noise. Images were processed using Leica confocal software.

## 2.7 Characterization of materials

Scanning electron microscopy (SEM) images were taken on a Quanta 450 scanning electron microscope. TEM observation was carried out on a Tecnai G2 Spirit transmission electron microscope at an acceleration voltage of 120 kV. Nitrogen adsorption-desorption isotherms were measured at -196 °C on a TriStar II surface area and porosity analyzer. The samples were degassed at 110 °C for 12 h before measurement. The Brunauer-Emmett-Teller (BET) specific surface areas (SBET) and the Barrett-Joyner-Halenda (BJH) pore-size distributions were derived from the adsorption branch of the isotherms. Thermogravimetric analysis of samples was performed on a S60/51920 TGA/DSC thermogravimetric analyzer using an oxygen flow of 30 ml/min and a heating ramp of 10 °C/min. Fluorescent emission and excitation spectra were recorded on a RF-5301PC spectrofluorophotometer (Shimadzu Scientific Instruments). Fourier transform infrared (FTIR) spectra of samples were recorded on a Thermo Scientific NICOLET 6700 spectrometer at room temperature. The dynamic light scattering (DLS) particle size distribution and zeta-potential of MSNs dispersed in H<sub>2</sub>O were measured using a Malvern Zetasizer Nano ZS (Malvern Inst. Ltd., U.K.) at room temperature. The pH of the suspension was adjusted with 0.1 M HCl or NaOH when necessary and monitored by a pH meter (EL20, METTLER TOLEDO).

## 3. Results and discussion

In this study, we first investigated separately the effects of using mixed surfactants, varying reaction temperature and reaction time, silica precursor quantity, and the catalyst concentration. Then, by analyzing the above results, summarized in Table 1, a mechanism for the particle formation is proposed. Finally, surface-functionalization of the stellate MSNs is demonstrated and the resulting composite nanoparticles are tested as intracellular drug delivery carriers.

### 3.1 Effect of mixed surfactants

From the SEM and TEM images in Fig. 1, it is clear that uniform nanoparticles can be synthesized using a mixture of

surfactants, CTAT and CTAB. Note that, for all the samples shown in the images, the total mole ratio of surfactant/TEOS is kept constant at 0.06. As the CTAT composition in the surfactant mixture increases from 0 (sample B10) to 100% (sample T10), the particle size increases gradually from about 50 to 110 nm. This effect on particle size will be discussed in more details after explaining the particle formation mechanism (section 3.6). Meanwhile, the appearance of the particle surface in the SEM images changes from smooth to a wrinkled surface with large pores, which appears on the particles synthesized at high CTAT content. The TEM images further confirm these particle structures after calcination, being discrete with little inter-particle aggregation.

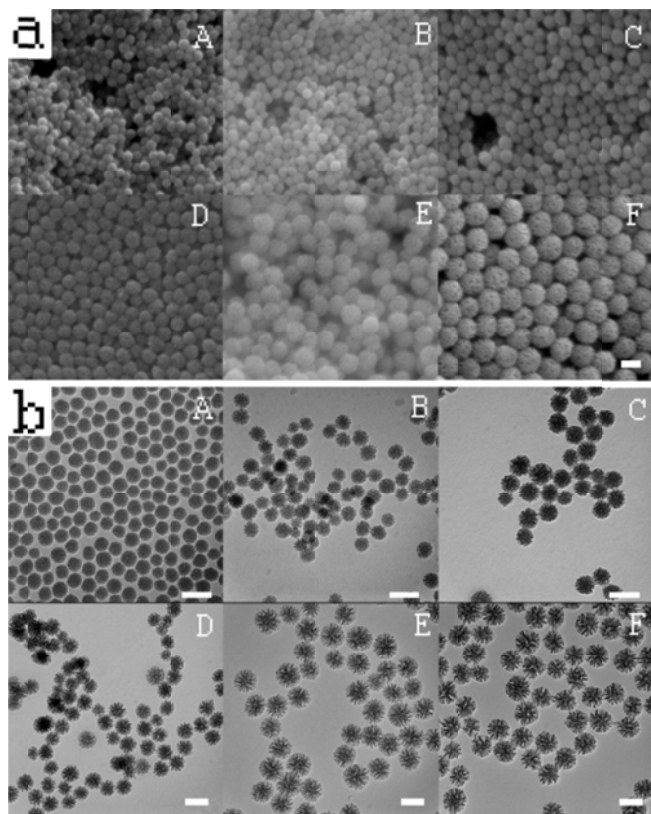


**Fig. 1** SEM (a) and TEM (b) images of MSN particles synthesized with mixed surfactants: (A) B10, (B) T3B7, (C) T5B5, (D) T7B3, (E) T9B1, (F) T10. Scale bars are 100 nm.

The nitrogen physisorption isotherms and the corresponding pore size distributions for these samples, shown in Fig. 2, demonstrate more clearly the evolution of the mesoporous structure with varying surfactant compositions. For B10, the narrow peak centered at 2 nm in the pore size distribution (PSD) curve originates from the cetyltrimethylammonium template and the broad peak around 40 nm is believed to be caused by inter-particle textural porosity. For T3B7 and T5B5, the PSD curves show peaks around 3 nm and this peak becomes broader with increasing CTAT content in the synthesis mixture. For T7B3, the peak around 3 nm remains, but another broad one centered around 10 nm also appears, suggesting the presence of a hierarchical porous structure. Although MSNs with hierarchical porous structure have been synthesized by using co-surfactant,<sup>32</sup> co-solvent<sup>33</sup> and/or organosilica precursors,<sup>34</sup> it is interesting to note that, it occurs in our case with two surfactants, CTAT and CTAB, consisting of the same

cetyltrimethylammonium cation (CTA<sup>+</sup>). In other words, this implies that, a hierarchical structure could be achieved by adjusting solely the anion nature of the surfactant. A further increase of the CTAT component leads to the presence of larger mesopores. T9B1 and T10 show pore sizes around 14 nm and 20 nm, respectively. The gradual enlargement of the mesopores with increasing CTAT content may be explained by an anion competition mechanism, as discussed before,<sup>28</sup> where the tosylate anions compete with silicate oligomers during the particle formation. One may speculate that, with increasing CTAT, more tosylate anions become incorporated into the as-prepared particles and larger mesopores are obtained after calcination. This hypothesis is supported partially by the thermogravimetry results for the surfactants (Fig. S2) and the as-prepared samples (Fig. S3). It is observed that as the CTAT increases in the synthesis mixture, the weight loss between 300 °C and 350 °C increases accordingly for the as-prepared samples. Although the decomposition of surfactant in mesoporous silica is a complex process involving multiple reactions and steps, the weight loss below 300 °C could mainly be attributed to the Hofmann degradation and fragmentation of CTA<sup>+</sup> binding to silica (SiO<sup>-</sup>).<sup>35</sup> On the other hand, the presence of CTA<sup>+</sup> in interactions with tosylate anions, that is, CTAT molecules, incorporated in the as prepared samples might contribute to the weight loss between 300 °C and 350 °C, which corresponds to organic components removed by oxidation.<sup>35</sup>

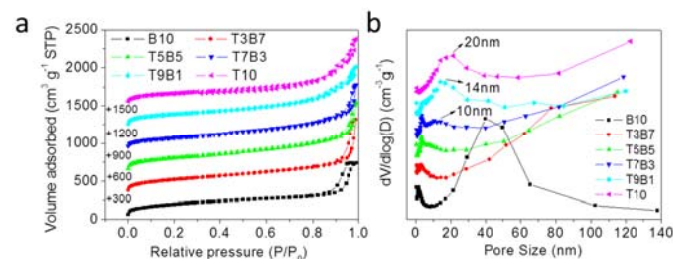


**Fig. 2** Nitrogen adsorption-desorption isotherms (a) and respective pore size distributions (b) of the various MSNs particles synthesized with mixed surfactants.

### 3.2 Effect of the reaction temperature

Fig. 3 shows SEM and TEM images of particles synthesized at various temperatures. Both the morphology viewed in SEM and the image contrast in TEM suggest an increase in particle porosity as the reaction temperature decreases from 95 °C to 50 °C. In terms of morphology, the particle sizes for T95, T80, and T65 are all around 110 nm, except for T50 which shows smaller a particle size of about 80 nm.

The nitrogen sorption results of these samples are shown in Fig. 4. All of the isotherms show a hysteresis loop at high relative pressure ( $P/P_0 > 0.9$ ), suggesting the existence of textural interparticle mesopores. The adsorbed volume measured below the relative pressure of 0.8, which can be attributed to the framework porosity, progressively increases with decreasing synthesis temperature. The most probable pore sizes of samples T95 and T80 are 8 nm and 20 nm, respectively, determined from the peak maximum of the PSD curves. For samples T65 and T50, although the most probable pore sizes are clearly above 20 nm, the exact values are difficult to ascertain because of the very broad distributions, which could be explained by the size overlap between the framework pores and the textural pores. Besides, T65 and T50 show significantly higher

framework pore volume than that of T80 and T95. These results are in good agreement with the observation from SEM and TEM analyses.

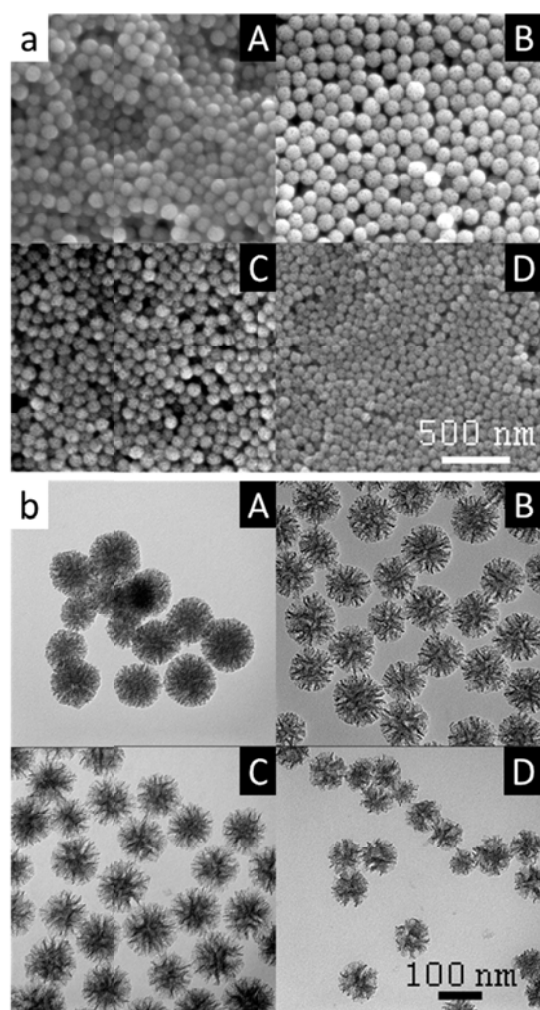


**Fig.3** SEM (a) and TEM (b) images of particles synthesized at various temperatures: (A) T95, (B) T80, (C) T65, (D) T50.

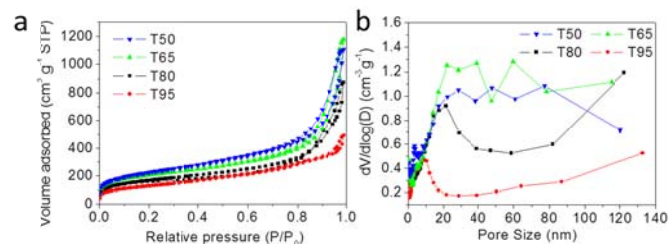


**Fig.4** Nitrogen adsorption-desorption isotherms (a) and respective pore size distributions (b) of particles synthesized at various temperatures.

The influence of reaction temperature can be explained in terms of the reaction kinetics. Lower temperature leads to lower reaction rate, which is also reflected by the product yield. The final yields of collected silica synthesized at 95 °C, 80 °C, 65 °C and 50 °C are 96%, 85%, 37% and 16%, respectively. This drastic decrease in the reaction rate with a decreasing temperature may lead to slower particle growth, and therefore, the particle size obtained at 50 °C would be significantly smaller than the other ones. On the other hand, a similar

particle size but with gradual decrease in pore volume in the order of T65, T80 and T95, indicates that a pore filling or contraction process may occur after the particle size reaches a critical value. These results suggest that reaction kinetics also play an important role influencing the formation of the large mesopores, in addition to the anion competition mechanism.

### 3.3 Effect of the reaction time

To clarify the influence of the reaction kinetics, samples were prepared at the same reaction temperature but subjected to different reaction times in order to analyze the particle evolution as a function of time.<sup>36, 37</sup> The reaction temperature is set at 35 °C for a slow reaction and thus, the ease of observation of different reaction stages.

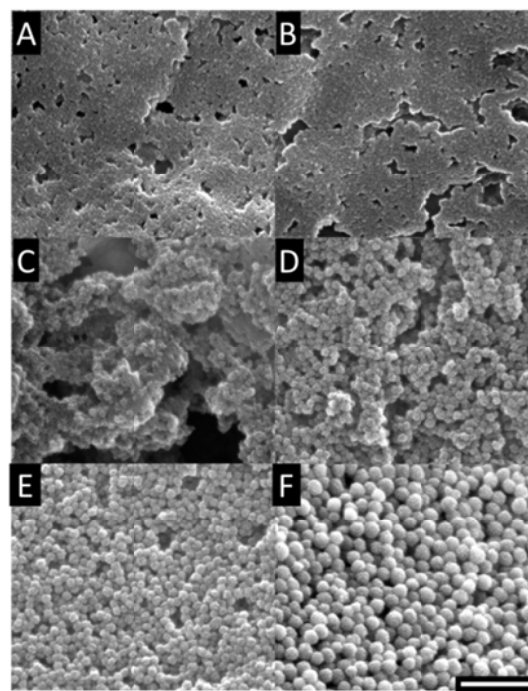


**Fig.5** SEM images of particles synthesized at 35 °C after (A) 0.5 h, (B) 1 h, (C) 2 h, (D) 4 h, (E) 6 h and (F) 24 h. Scale bar is 500 nm.

SEM images of the products from 0.5 h to 24 h reaction are shown in Fig. 5. No discrete particles could be identified in the 0.5 h and 1 h products, and only some wrinkled structures appeared in the 2 h product. It should be noted that after 2 h reaction, the two immiscible phases of H<sub>2</sub>O/TEOS can still be distinguished if stirring was stopped. This suggests the particles are not formed in a homogeneous system but in a system more similar to that used to prepare silica nanoparticles from basic amino acids.<sup>37, 38</sup> This kind of two-phase synthesis was reported to contribute to the monodispersity of the final particles.<sup>39</sup> After 4 h reaction, uniform particles of 50 nm become identifiable and their size increases slightly up to about 60 nm after 6 h. Finally, spherical particles of 100 nm with large pores on their surface are obtained after 24 h. Meanwhile, the particles obtained after different reaction periods at 35 °C were analyzed by nitrogen sorption to monitor the pore size evolution (Fig. S4). While the sample obtained at 6 h shows pore size around 20 nm, the samples obtained beyond 12 h show almost constant pore size about 12 nm. Because uniform-sized silica particles are obtained regardless of the reaction time from 4 h to 24 h, it can be inferred that only particle growth occurs at this stage

without new particle nucleation/formation. The particle growth period was also observed for reaction at other temperatures. From 2 h to 24 h at 50 °C, the particle size increases from 80 nm for T50 sample to 100 nm for T50-24h sample (Fig. S5). Thus, we assume that, the reaction follows a nucleation-growth mechanism. Besides, it is interesting to note that the prolonged reaction time at 50 °C also leads to reduced framework pore volume and pore size (Fig. S5), which is consistent with the particle evolution at 35 °C and corresponds well to the kinetic effect of different reaction temperatures.

### 3.4 Effect of the silica precursor quantity

If a nucleation-growth process accurately describes the particle formation mechanism, it should be reasonable that the particle size can be directly controlled by changing the quantity of silica precursor. To verify this hypothesis, the sample TSi/3 was synthesized using 1/3 TEOS amount of the formula for T10. Here, it was expected that the usage of reduced silica precursor should lead to decreased particle size, because fewer silicate species would participate in the particle growth process.

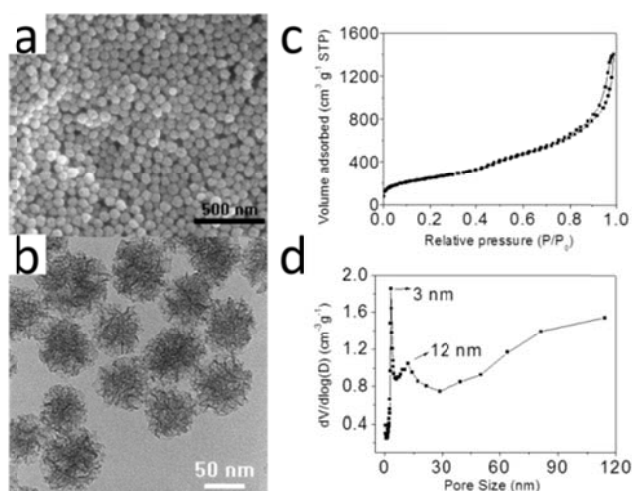


**Fig.6** SEM (a), TEM (b) image, nitrogen adsorption-desorption isotherm (c) and pore size distribution curve (d) of TSi/3.

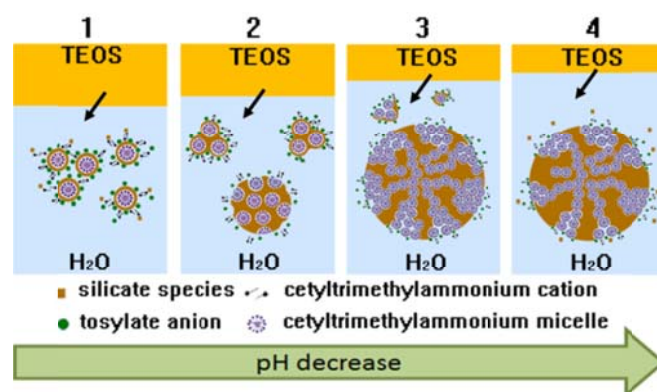
The characterization results of TSi/3 in Fig. 6 are consistent with our expectation. This sample is also constituted of relatively uniform nanoparticles. However, the particle size of TSi/3 is around 70 nm and significantly smaller than that of T10, which shows a particle size around 110 nm (see Fig. 1). Besides, large mesopores around 10 nm are also observed on the particle surface from the SEM investigations. Furthermore, the PSD clearly indicates that, in addition to the large mesopores represented by the peak at 12 nm, a significant amount of 3 nm mesopores also exist in this sample. From the SEM and TEM observations, these 3 nm mesopores are more likely to be located in the inner part of the particles, indicating they are essentially formed at early stage of the particle formation. It is documented that the pH in the MSN synthesis mixture declines as the silica condensation proceeds.<sup>17, 38</sup> Therefore, this hierarchical structure may be justified by the pH variation and anion competition during the reaction process. At the beginning of the reaction, the pH of the system is high (above 11) so that the tosylate anion dissociates easily from CTA<sup>+</sup> cation. Under these conditions, normal 3 nm CTA<sup>+</sup>/silicate micelles are formed and aggregate into a

mesophase to form the primary particles. As the reaction proceeds and the pH drops to near neutral, binding of tosylate to CTA<sup>+</sup> will eventually become strong enough to compete with silicate species, and from this time larger mesopores will begin to develop due to the incorporation of the tosylate anions.

### 3.5 Effect of the catalyst concentration

The catalyst amount is an important factor in determining both the particle size and the pore structure of TEA-derived silica.<sup>18</sup> Although the effect of TEA/TEOS ratios (from 8 to 0.026) has been studied,<sup>28</sup> this work emphasizes that 0.026 is not the lowest limit. Stellate nanoparticles with large surface pores can still be successfully synthesized at much lower TEA/TEOS ratios of 0.013 and 0.0065, but the particle sizes increase slightly to 130~150 nm (Fig. S6). Interestingly, another study also reported that lower TEA catalyst quantity could result in larger MSNs when CTAB is used as the surfactant.<sup>5</sup> Based on a nucleation-growth model, it can be suggested that at low TEA concentration, the hydrolysis rate of TEOS is limited, leading to fewer primary particles formed in the initial period, which then further grow into larger particles. Meanwhile, owing to the very low base concentration used, the pH of the reaction mixture may decrease so quickly that particle nucleation can only occur in the short initial period. Afterwards, during the prolonged growth stage, the particles gradually grow in size and become spherical in shape, as demonstrated in Fig. 5. However, when we try to further increase the particle size by reducing TEA/TEOS ratio to 0.00325, some smaller particles of several tens nanometer are present accompanied by large pore spheres above 100 nm. When no TEA was added at all, only aggregated irregular particles that are smaller than 40 nm were obtained. These irregular particles present low surface area and almost only textural porosity (Fig. S7), which could be attributed to the weak interactions between silicate species and the surfactant template. Therefore, it can be concluded that there is a very low, but critical, base concentration, below which stellate MSNs cannot be obtained.

### 3.6 Proposed mechanism for particle formation



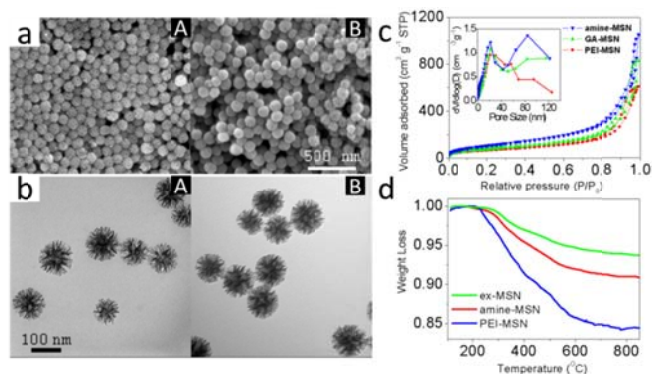
**Scheme 2** Scheme for the proposed formation process of stellate MSNs.

Based on the above analysis of the effects of different synthesis parameters, a possible formation mechanism for the stellate MSNs is proposed in Scheme 2. The whole process can be divided into 4 stages: 1) TEOS molecules diffuse into the water phase and become hydrolyzed into silicate species.

Following condensation processes, the oligomeric silicate species assemble with  $\text{CTA}^+$  cations, through adsorption, to form hybrid micelles via the S<sup>T</sup> (S: surfactant; I: inorganic species) pathway; 2) Several hybrid micelles aggregate and form primary particles; 3) Due to the decrease of pH, partly silylated micelles begin to form, as tosylate anions compete with silicate for  $\text{CTA}^+$ . These partly silylated micelles add to the primary particles and result in particle growth and the formation of large mesopores. 4) With the further decrease of pH, the interactions between silicate species and  $\text{CTA}^+$  become even weaker. The continuous deposit of silicate species into the large mesopores should lead then to decrease in particle porosity. In this nucleation-growth model, the final particle size is greatly influenced by the number of nuclei/primary particles formed at the initial reaction period. When CTAB is replaced by CTAT in the mixed surfactant system, the amount of free  $\text{CTA}^+$  cations in the reaction medium could become lower due to the stronger binding of tosylate over bromide towards  $\text{CTA}^+$ . Because the nucleation is promoted by forming hybrid micelles between  $\text{CTA}^+$  and silicate species, fewer free  $\text{CTA}^+$  cations may lead to fewer nuclei and thus larger final particle sizes, as demonstrated in Fig. 1.

### 3.7 Surface functionalization and delivery application

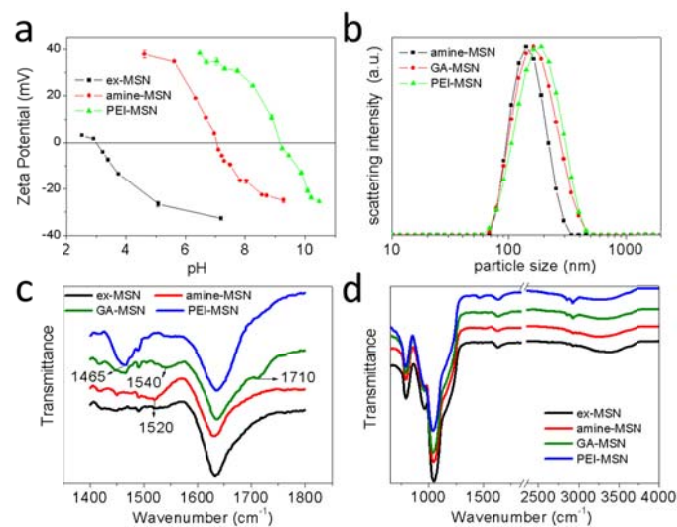
An important advantage of MSNs as a drug delivery platform is their tunable surface chemistry and the ease of conjugation with various functional groups.<sup>40</sup> In this study, a nontoxic low molecular weight branched PEI (800 Da) was conjugated to the above large pore stellate MSNs to form an intracellular DOX-delivery system, because PEI has been proven to enhance cellular uptake,<sup>41</sup> dispersion at physiologic pH,<sup>42</sup> and endosome escape<sup>43</sup> of MSNs. Although the functionalization with large organic groups often leads to pore blocking/saturation,<sup>9</sup> large mesopore structure was reported to alleviate this problem.<sup>44,45</sup> Furthermore, by taking advantage of the particle growth process, a delayed condensation method<sup>31</sup> can readily be applied to selectively functionalize the external part of the particles, while leave the inner part mostly unmodified to interact with the DOX molecules.



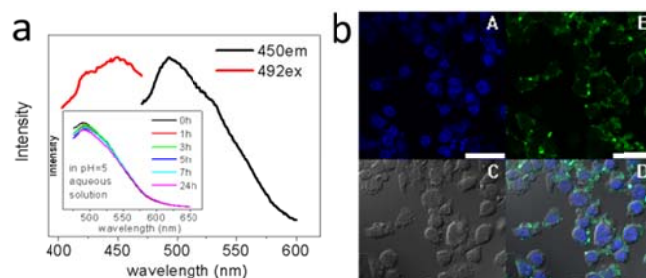
**Fig. 7** SEM (a) and TEM (b) images of (A) amine-MSN and (B) PEI-MSN. Nitrogen adsorption-desorption isotherms with respective pore size distributions inserted (c) and thermogravimetric curves (d) of the functionalized MSNs.

Fig. 7a and 7b show the SEM and TEM images of amine- and PEI-modified particles. By comparing amine-MSNs with the previous T10 sample, it can be concluded that the delayed co-condensation with APTES does not change the particle size and morphology significantly. After further PEI modification,

there is a visible reduction of surface porosity due to the PEI coating, which was confirmed by nitrogen sorption measurements (Fig 7c). The increased organic content of functionalized particles is also reflected in TGA measurement, as shown in Fig 7d. The weight loss from 110 °C to 850 °C for ex-MSN, amine-MSN and PEI-MSN are 6%, 9% and 15%, respectively.



**Fig. 8** Zeta potential (a), DLS size distributions (b) and FTIR spectra (c) of functionalized MSNs. The spectra in (d) are the enlarged part of (c).



**Fig. 9** (a) Emission and excitation fluorescence spectra of PEI-MSN. “em450” indicates an emission at 450 nm excitation. Similarly, “ex492” stands for an excitation spectrum at 492 nm detection. The insert is the emission spectra at 450 nm excitation obtained after incubation in pH=5 aqueous solution for various times. (b) CLSM images of HeLa cells after incubation with 50 μg/ml PEI-MSN for 3 h. Image (D) is the merged picture of blue channel from Hoechst (A), green channel from PEI-MSN (B), and the differential interference contrast channel (C). Scale bars are 50 μm.

The successful surface functionalization was further confirmed by surface zeta potential measurement and FTIR. In Fig. 8a, while unmodified ex-MSNs show an isoelectrical point (IEP) around 3, amine-MSNs and PEI-MSNs show IEP of nearly 7 and 9, respectively. The increase in IEP reflects the increase of surface amine groups. Besides, a slight increase in the particle size after functionalization can be identified from the DLS size distributions shown in Fig. 8b. The average particle sizes determined by DLS for ex-MSNs, amine-MSNs and PEI-MSNs are 154 nm, 168 nm and 202 nm, respectively. These sizes are larger than those observed in TEM, which could be due to the surface hydration layer and/or slight aggregation in solution. This kind of deviation was also observed in several

other studies.<sup>4, 18</sup> In the FTIR spectra shown in Fig. 8c, all of the particles show typical peaks corresponding to silica around 789  $\text{cm}^{-1}$ , 960  $\text{cm}^{-1}$  and 1040  $\text{cm}^{-1}$ , which are attributed to the symmetric Si-O, Si-OH and asymmetric Si-O-Si vibrations, respectively. The peak around 1630  $\text{cm}^{-1}$  is due to physisorbed water.<sup>30</sup> However, in the range of 1400-1600  $\text{cm}^{-1}$  shown in Fig. 8d, the unmodified ex-MSNs show no peak while amine-MSNs show a peak around 1520  $\text{cm}^{-1}$  which is assigned to N-H bending.<sup>30</sup> After conjugation of the amine-MSN with the glutaraldehyde linker, two peaks around 1540  $\text{cm}^{-1}$  and 1710  $\text{cm}^{-1}$  appear, which can be attributed to C=C and C=O in glutaraldehyde and its oligomer.<sup>46</sup> Note that, the characteristic band of C=N occurs around 1640  $\text{cm}^{-1}$  and may be masked by the 1630  $\text{cm}^{-1}$  band of water. However, the change of the powder color from white to yellow (Fig. S8) suggests the formation of a Schiff bond.<sup>47</sup> After the reaction with PEI, a peak around 1465  $\text{cm}^{-1}$  corresponding to C-H bending appears, which is accompanied by an increase of the C-H stretching band in 2800-3000  $\text{cm}^{-1}$ .

Interestingly, the PEI-MSN particles show auto-fluorescence without additional fluorescent label, as shown by the emission and excitation spectra in Fig. 9. Similar auto-fluorescence has previously been reported<sup>46, 48</sup> using aldehyde as crosslinker between amine groups, and it was attributed to the  $n-\pi^*$  transition of the C=N bonds in the Schiff's base. In addition, to test the possibility of using this auto-fluorescence for tracking particles in intracellular delivery, the fluorescence stability of PEI-MSN in a pH=5 aqueous solution was checked because both the extracellular tumor microenvironment and the endosome/lysosome organelles exhibit mild acidic pH.<sup>49</sup> Although Schiff bases are usually unstable under acidic conditions, the fluorescence intensity of PEI-MSN remained stable up to 24 h as shown in Fig. 9a (insert), which could be attributed to the exceptional stability of the cross-linking formed by glutaraldehyde.<sup>50</sup> Confocal microscope images (Fig. 9b) confirm the green fluorescence of PEI-MSNs in cell culture.

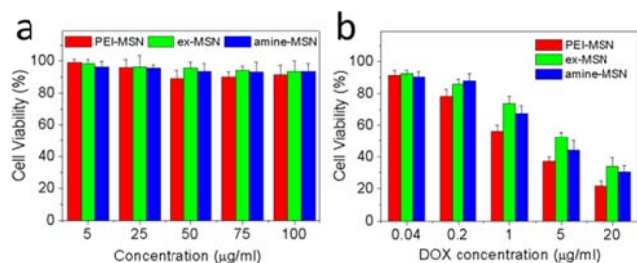


**Fig. 10** Hela cell viabilities after 24 h of incubation with MSNs (a) and DOX-loaded MSNs (b).

Following this, DOX was loaded into PEI-MSN, amine-MSN and ex-MSN and the loading efficiencies determined by UV-vis adsorption using a standard curve (Fig. S9) were 21%, 26%, 30%, respectively, which is consistent with the increasing order of pore volume. The resulting DOX-loaded particles exhibited sustained and pH-dependent release behavior owing to the increased solubility of DOX at low pH (Fig. S10). In the MTT tests shown in Fig. 10, all the three types of particle showed good biocompatibility below a particle concentration of 100  $\mu\text{g/ml}$  with cell viability above 80%. On the other hand, PEI-MSN showed higher inhibition efficacy towards Hela cells than amine-MSN and ex-MSN after DOX loading, which could be attributed to the enhanced cell uptake of the nanoparticles with the surface PEI modification.<sup>41</sup> The successful delivery of

DOX by PEI-MSN was verified by confocal microscopy (Fig. S11) and the delivery process was monitored up to 24 h (Fig. S12). We observed that, there is already significant DOX accumulation in Hela cell cytoplasm after 1 h incubation with PEI-MSN, suggesting efficient cell uptake. The DOX-loaded particles are mainly located at the periphery of cell nuclei. After 4 h, the DOX concentration in the cytoplasm increases further. After 12 h, DOX diffusion into the cell nucleus can be observed. After 24 h, almost all DOX has been translocated to the cell nucleus, where it plays its anticancer role. These results demonstrate PEI-MSN has excellent potential as an intracellular drug delivery system.

#### 4. Conclusions

In summary, stellate MSNs with 50-140 nm particle size and 2-20 nm pore size are obtained easily by choosing proper synthesis parameters. The particle formation follows a nucleation-growth process, in which the reaction kinetics greatly influences particle size and mesoporous structure of the final products. Taking into account that parameters, such as the surfactant composition, reaction temperature and time, and reactant ratio, can be adjusted continuously, it is reasonable to deduce that both the particle size and the pore structure can be tailored accordingly. Moreover, these MSNs can be suitably modified with biofunctional groups/molecules, e.g. nontoxic low molecular weight PEI, and have demonstrated good intracellular delivery capability. Therefore, the excellent flexibility of the structure and surface chemistry endow these stellate MSNs wide prospect in drug delivery applications and will also facilitate further study on various size/structure-dependent nanoparticle-cell interactions.

#### Acknowledgements

This work was financially supported by the Australian Research Council (ARC) through the Discovery Project program (DP130104459 and DP140104062). Lin Xiong acknowledges a scholarship from The University of Adelaide.

#### Notes and references

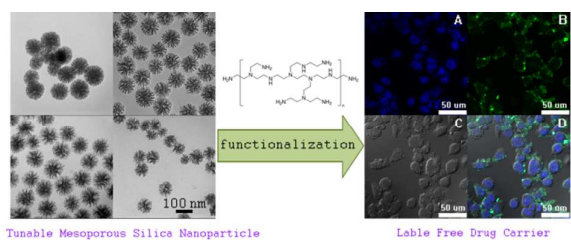
<sup>a</sup> School of Chemical Engineering, The University of Adelaide, Adelaide, SA 5005, Australia. E-mail: s.qiao@adelaide.edu.au. Fax: +61 8 8303 4373. Tel: +61 8 8313 6443.

<sup>b</sup> Department of Chemistry and Centre de Recherche sur les Matériaux Avancés (CERMA), Université Laval, Quebec City, QC G1V 0A6, Canada.

† Electronic Supplementary Information (ESI) available: [surface reaction, TGA, TEM, SEM, nitrogen adsorption-desorption, calibration curve, drug release profile and confocal microscopy]. See DOI: 10.1039/b000000x/

- 1 Q. He and J. L. Shi, *Adv. Mater.*, 2014, **26**, 391-411.
- 2 C. Argyo, V. Weiss, C. Bräuchle and T. Bein, *Chem. Mater.*, 2014, **26**, 435-451.
- 3 Q. He, Z. Zhang, F. Gao, Y. Li and J. L. Shi, *Small*, 2011, **7**, 271-280.
- 4 F. Lu, S.-H. Wu, Y. Hung and C.-Y. Mou, *Small*, 2009, **5**, 1408-1413.

- 5 L. Pan, Q. He, J. Liu, Y. Chen, M. Ma, L. Zhang and J. L. Shi, *J. Am. Chem. Soc.*, 2012, **134**, 5722-5725.
- 6 Y.-S. Lin and C. L. Haynes, *J. Am. Chem. Soc.*, 2010, **132**, 4834-4842.
- 7 Y. Gao, Y. Chen, X. Ji, X. He, Q. Yin, Z. Zhang, J. L. Shi and Y. Li, *ACS Nano*, 2011, **5**, 9788-9798.
- 8 A. Popat, J. Liu, Q. Hu, M. Kennedy, B. Peters, G. Q. Lu and S. Z. Qiao, *Nanoscale*, 2012, **4**, 970-975.
- 9 M. Bouchoucha, R. C.-Gaudreault, M.-A. Fortin and F. Kleitz, *Adv. Funct. Mater.*, 2014, **24**, 5911-5923.
- 10 W. Stöber, A. Fink and E. Bohn, *J. Colloid Interf. Sci.*, 1968, **26**, 62-69.
- 11 Q. Cai, Z.-S. Luo, W.-Q. Pang, Y.-W. Fan, X.-H. Chen and F.-Z. Cui, *Chem. Mater.*, 2001, **13**, 258-263.
- 12 R. I. Nooney, D. Thirunavukkarasu, Y. Chen, R. Josephs and A. E. Ostafin, *Chem. Mater.*, 2002, **14**, 4721-4728.
- 13 C. E. Fowler, D. Khushalani, B. Lebeau and S. Mann, *Adv. Mater.*, 2001, **13**, 649-652.
- 14 Y. Han and J. Y. Ying, *Angew. Chem. Int. Ed.*, 2005, **44**, 288-292.
- 15 K. Suzuki, K. Ikari and H. Imai, *J. Am. Chem. Soc.*, 2004, **126**, 462-463.
- 16 J. Gu, W. Fan, A. Shimojima and T. Okubo, *Small*, 2007, **3**, 1740-1744.
- 17 Z.-A. Qiao, L. Zhang, M. Guo, Y. Liu and Q. Huo, *Chem. Mater.*, 2009, **21**, 3823-3829.
- 18 K. Möller, J. Kobler and T. Bein, *Adv. Funct. Mater.*, 2007, **17**, 605-612.
- 19 L. Jia, J. Shen, Z. Li, D. Zhang, Q. Zhang, C. Duan, G. Liu, D. Zheng, Y. Liu and X. Tian, *Int. J. Pharm.*, 2012, **439**, 81-91.
- 20 H. S. Shin, Y. K. Hwang and S. Huh, *ACS Appl. Mater. Interfaces*, 2014, **6**, 1740-1746.
- 21 I. I. Slowing, B. G. Trewyn and V. S. Y. Lin, *J. Am. Chem. Soc.*, 2007, **129**, 8845-8849.
- 22 S. B. Hartono, W. Gu, F. Kleitz, J. Liu, L. He, A. P. Middelberg, C. Yu, G. Q. Lu and S. Z. Qiao, *ACS Nano*, 2012, **6**, 2104-2117.
- 23 Y. Chen, C. Chu, Y. Zhou, Y. Ru, H. Chen, F. Chen, Q. He, Y. Zhang, L. Zhang and J. L. Shi, *Small*, 2011, **7**, 2935-2944.
- 24 D. Niu, Z. Ma, Y. Li and J. L. Shi, *J. Am. Chem. Soc.*, 2010, **132**, 15144-15147.
- 25 M. Mizutani, Y. Yamada, T. Nakamura and K. Yano, *Chem. Mater.*, 2008, **20**, 4777-4782.
- 26 F. Gao, P. Botella, A. Corma, J. Blesa and L. Dong, *The Journal of Physical Chemistry B*, 2009, **113**, 1796-1804.
- 27 M.-H. Kim, H.-K. Na, Y.-K. Kim, S.-R. Ryoo, H. S. Cho, K. E. Lee, H. Jeon, R. Ryoo and D.-H. Min, *ACS Nano*, 2011, **5**, 3568-3576.
- 28 K. Zhang, L.-L. Xu, J.-G. Jiang, N. Calin, K.-F. Lam, S.-J. Zhang, H.-H. Wu, G.-D. Wu, B. Albel, L. Bonneviot and P. Wu, *J. Am. Chem. Soc.*, 2013, **135**, 2427-2430.
- 29 V. Polshettiwar, D. Cha, X. Zhang and J. M. Basset, *Angew. Chem. Int. Ed.*, 2010, **49**, 9652-9656.
- 30 X. Du and J. He, *Nanoscale*, 2012, **4**, 852-859.
- 31 J. Kecht, A. Schlossbauer and T. Bein, *Chem. Mater.*, 2008, **20**, 7207-7214.
- 32 H. Djojoputro, X. F. Zhou, S. Z. Qiao, L. Z. Wang, C. Z. Yu and G. Q. Lu, *J. Am. Chem. Soc.*, 2006, **128**, 6320-6321.
- 33 X. Du and J. He, *Langmuir*, 2011, **27**, 2972-2979.
- 34 Y. Chen, H. Chen, M. Ma, F. Chen, L. Guo, L. Zhang and J. L. Shi, *J. Mater. Chem.*, 2011, **21**, 5290.
- 35 F. Kleitz, W. Schmidt and F. Schüth, *Micropor. Mesopor. Mat.*, 2001, **44-45**, 95-109.
- 36 T. Suteewong, H. Sai, M. Bradbury, L. A. Estroff, S. M. Gruner and U. Wiesner, *Chem. Mater.*, 2012, **24**, 3895-3905.
- 37 T. Yokoi, J. Wakabayashi, Y. Otsuka, W. Fan, M. Iwama, R. Watanabe, K. Aramaki, A. Shimojima, T. Tatsumi and T. Okubo, *Chem. Mater.*, 2009, **21**, 3719-3729.
- 38 T. Yokoi, T. Karouji, S. Ohta, J. N. Kondo and T. Tatsumi, *Chem. Mater.*, 2010, **22**, 3900-3908.
- 39 J. Wang, A. Sugawara-Narutaki, M. Fukao, T. Yokoi, A. Shimojima and T. Okubo, *ACS Appl. Mater. Interfaces*, 2011, **3**, 1538-1544.
- 40 J. L. Vivero-Escoto, I. I. Slowing, B. G. Trewyn and V. S. Y. Lin, *Small*, 2010, **6**, 1952-1967.
- 41 T. Xia, M. Kovoichich, M. Liong, H. Meng, S. Kabehie, S. George, J. I. Zink and A. E. Nel, *ACS Nano*, 2009, **3**, 3273-3286.
- 42 J. M. Rosenholm, A. Meinander, E. Peuhu, R. Niemi, J. E. Eriksson, C. Sahlgren and M. Lindén, *ACS Nano*, 2009, **3**, 197-206.
- 43 C. Hom, J. Lu, M. Liong, H. Luo, Z. Li, J. I. Zink and F. Tamanoi, *Small*, 2010, **6**, 1185-1190.
- 44 A. Martin, G. Morales, F. Martinez, R. van Grieken, L. Cao and M. Kruk, *J. Mater. Chem.*, 2010, **20**, 8026-8035.
- 45 A. Martín, R. A. García, D. S. Karaman and J. M. Rosenholm, *J. Mater. Sci.*, 2013, **49**, 1437-1447.
- 46 W. Wei, L. Y. Wang, L. Yuan, Q. Wei, X. D. Yang, Z. G. Su and G. H. Ma, *Adv. Funct. Mater.*, 2007, **17**, 3153-3158.
- 47 T. G. Waddell, D. E. Leyden and M. T. DeBello, *J. Am. Chem. Soc.*, 1981, **103**, 5303-5307.
- 48 Z. Wang, H. Zhu, D. Li and X. Yang, *Colloid Surface. A*, 2008, **329**, 58-66.
- 49 E. S. Lee, Z. Gao and Y. H. Bae, *J. Control Release.*, 2008, **132**, 164-170.
- 50 I. Migneault, C. Dartiguenave, M. J. Bertrand and K. C. Waldron, *Biotechniques.*, 2004, **37**, 790-806.



Tunable Mesoporous Silica Nanoparticle

Label Free Drug Carrier

Tunable stellate mesoporous silica nanoparticles are functionalized with low molecular poly(ethylene imine) for efficient label-free intracellular drug delivery.